# Effect of an imperfect interface in a quartz crystal microbalance for detecting the properties of an additional porous layer

Peng Li and Feng Jin

Citation: Journal of Applied Physics **115**, 054502 (2014); doi: 10.1063/1.4862559
View online: http://dx.doi.org/10.1063/1.4862559
View Table of Contents: http://aip.scitation.org/toc/jap/115/5
Published by the American Institute of Physics

# Effect of an imperfect interface in a quartz crystal microbalance for detecting the properties of an additional porous layer

Peng Li and Feng Jin[a)]
*State Key Laboratory for Strength and Vibration of Mechanical Structures, School of Aerospace, Xi'an Jiaotong University, Xi'an 710049, People's Republic of China*

(Received 1 November 2013; accepted 7 January 2014; published online 3 February 2014)

Sauerbrey's equation may yield incorrect results when the upper layer is not rigidly attached onto the quartz crystal plate. Thus, we investigate the effect of an imperfect interface on the anti-plane vibration of a quartz crystal microbalance for detecting the characteristics of the upper transversely isotropic porous layer. Both the stiffness and inertial effect of the porous layer, as well as the influence of an inhomogeneous interface, are considered for an infinite or finite AT-cut (35°15′ cut deviating principal optic axis) quartz plate. The appearance of a weak interface is theoretically and numerically revealed to excite a new thickness twist wave in an infinite quartz crystal plate. Meanwhile, the non-uniform interface evidently changes the displacement and stress distributions, which is totally different from the homogeneous interface. These findings prove effective guidance for physical phenomenon explanations and experimental measurement in mass sensor devices.  [http://dx.doi.org/10.1063/1.4862559]

## I. INTRODUCTION

A quartz crystal microbalance (QCM) is usually a quartz plate or disk that is widely used to measure the characteristics of an additional thin layer upon its surface.[1] Specifically, when a thin layer of another material is added to the crystal surface, its resonant frequencies become lower mainly due to inertia. Using this property, a QCM has been successfully applied to detect the micro-mass changes, as well as the chemical, biological and physical properties of thin layers deposited on it.[2–4]

A porous medium is a material containing pores that are typically filled with a fluid (liquid or gas), which has important applications in sensor devices[5] because of its particular advantage of having very high area compared with a solid deposit. For example, the energy losses in the GHz range and forward reflection coefficient characteristics of a thin-film bulk acoustic wave resonator can be improved by using a porous silicon layer etching in the ZnO/Si composites.[6] The sensitivity of the quartz crystal microbalances for QCM can be enhanced evidently by replacing the conventional electrode with porous alumina[7] and gold electrodes.[8] Furthermore, the refractive index can be lowered in the visible optical region if the porosity of the porous anodic aluminum oxide thin films embedded on the quartz substrate is chosen properly.[9] Most of the works about QCM with a porous material are based on experimental equipment. To the best of our knowledge, systematic theoretical investigations about the application of porous material in QCM, which can provide physical phenomena explanations and guidance for experimental measurements, are still lacking.

Meanwhile, Sauerbrey's equation provides linear relationship between the resonance frequency shift of QCM and the mass attached on the surface.[10] Only the inertia of the additional layer is considered, and its stiffness effect has been ignored in this equation for simplification. However, Sauerbrey's equation may yield incorrect results, especially when the additional mass layer is not attached rigidly,[11] which limit its practical application. Therefore, the present study investigates the anti-plane vibration of quartz crystal plate with a porous layer imperfectly bonded on its surface. Both the stiffness and the inertial effects are included, which may compensate the deficiency of Sauerbrey's equation to some extent.

The shear horizontal (SH) or anti-plane vibration is solved for an infinite AT-cut quartz plate using Mindlin's solution.[12,13] This frequency equation can be reduced to some previous classical outcomes for some special cases. A new thickness twist wave, excited by imperfect interface, is revealed through approximation analysis and perturbation method. This kind of wave disappears when the interface becomes perfect. Ignoring the small coupling coefficient $c_{56}$, the solutions of the finite crystal plate are obtained using the trigonometric function expansion technique. Different from that of a previous work,[14,15] the interface is inhomogeneous along the plate length direction. The frequency shift, as well as the displacement and stress distributions, is examined, and some conclusions are achieved.

## II. BASIC EQUATIONS

A transversely isotropic porous layer with a thickness $2h_0$ imperfectly bonded on an infinite AT-cut quartz plate whose thickness is $2h$ is shown in Figure 1. A particular cut of a crystal plate refers to the orientation of the plate when taken out of an anisotropic bulk crystal. As a consequence, crystal plates with different cuts exhibit different anisotropies in the coordinates that are normal and parallel to the plate surfaces. The widely used AT-cut quartz plate is a special case of rotated Y-cut quartz plate that is effectively monoclinic in the plate coordinate system. Meanwhile, quartz has very weak piezoelectric coupling;[16] thus, for free

[a)]Author to whom correspondence should be addressed. Electronic mail: jinfengzhao@263.net. Fax: +86-29-82667091.

 

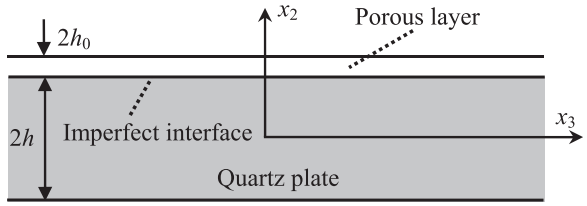


FIG. 1. A QCM containing of a uniform porous layer imperfectly attached on an infinite AT-cut quartz plate.

vibration frequency analysis, this small piezoelectric coupling can be neglected and an elastic analysis is sufficient.

In the following equations, the parameters with a superscript "′" symbol represent variables in the porous layer. In addition, the body forces and the viscosity of the upper fluid-saturated layer are ignored. Following Biot's theory,[17] the governing equations of quartz plate and porous layer can be expressed as follows:

$$T_{ij,j} = \rho \ddot{u}_i, \tag{1a}$$

$$T'_{ij,j} = \rho_{11}\ddot{u}'_i + \rho_{12}\ddot{U}'_i,\ \sigma'_{,i} = \rho_{12}\ddot{u}'_i + \rho_{22}\ddot{U}'_i, \tag{1b}$$

where a comma followed by subscript $i$ denotes differentiation with respect to the corresponding coordinate, and the dot refers to time differentiation. $T_{ij}$, $u_i$, and $\rho$ are the components of the stress, displacement and mass density of the crystal plate, respectively. For the porous layer, $u'_i$ are the components of the solid phase displacements, and $U'_i$ are those of the fluid phase displacements. $\sigma' = -\beta p$ is the reduced pressure of the fluid ($p$ is the pressure in the fluid and $\beta$ is the porosity of the medium). Mass coefficients $\rho_{11}$, $\rho_{22}$, $\rho_{12}$ account for the inertias of the solid and fluid phases, and the effects of the momentum transfer between the two phases. Moreover, these coefficients obey the following inequalities:[17]

$$\rho_{11} > 0, \quad \rho_{22} > 0, \quad \rho_{12} < 0, \quad \rho_{11}\rho_{22} - \rho_{12}^2 > 0. \tag{2}$$

The constitutive equations corresponding to quartz plate and the porous layer can be expressed as follows:[17,18]

$$T_{ij} = c_{ijkl}\varepsilon_{kl}, \tag{3a}$$

$$T'_{ij} = c'_{ijkl}\varepsilon'_{kl} + m'_{ij}E',\quad \sigma' = m'_{ij}\varepsilon'_{ij} + R'E', \tag{3b}$$

where $c_{ijkl}$ $(c'_{ijkl})$ and $\varepsilon_{kl}$ $(\varepsilon'_{kl})$ are the components of the elastic coefficient and strain tensors in the crystal plate (porous layer), respectively, and $m'_{ij}$ and $R'$ are the material parameters in the porous layer. Moreover, the geometric equations in the quartz plate and the porous layer can be written as follows:[17]

$$\varepsilon_{ij} = \frac{1}{2}(u_{i,j} + u_{j,i}), \tag{4a}$$

$$\varepsilon'_{ij} = \frac{1}{2}\left(u'_{i,j} + u'_{j,i}\right),\ E' = U'_{i,i}. \tag{4b}$$

The constitutive equations of (3) can be represented in terms of components as follows:[17–19]

$$\begin{Bmatrix} T_{11} \\ T_{22} \\ T_{33} \\ T_{23} \\ T_{13} \\ T_{12} \end{Bmatrix} = \begin{bmatrix} c_{11} & c_{12} & c_{13} & c_{14} & 0 & 0 \\ c_{12} & c_{22} & c_{23} & c_{24} & 0 & 0 \\ c_{13} & c_{23} & c_{33} & c_{34} & 0 & 0 \\ c_{14} & c_{24} & c_{34} & c_{44} & 0 & 0 \\ 0 & 0 & 0 & 0 & c_{55} & c_{56} \\ 0 & 0 & 0 & 0 & c_{56} & c_{66} \end{bmatrix} \begin{Bmatrix} \varepsilon_{11} \\ \varepsilon_{22} \\ \varepsilon_{33} \\ 2\varepsilon_{23} \\ 2\varepsilon_{13} \\ 2\varepsilon_{12} \end{Bmatrix} \tag{5a}$$

and

$$\begin{Bmatrix} T'_{11} \\ T'_{22} \\ T'_{33} \\ T'_{23} \\ T'_{13} \\ T'_{12} \\ \sigma' \end{Bmatrix} = \begin{bmatrix} c'_{11} & c'_{12} & c'_{13} & 0 & 0 & 0 & m'_{11} \\ c'_{12} & c'_{11} & c'_{13} & 0 & 0 & 0 & m'_{11} \\ c'_{13} & c'_{13} & c'_{33} & 0 & 0 & 0 & m'_{33} \\ 0 & 0 & 0 & c'_{44} & 0 & 0 & 0 \\ 0 & 0 & 0 & 0 & c'_{44} & 0 & 0 \\ 0 & 0 & 0 & 0 & 0 & c'_{66} & 0 \\ m'_{11} & m'_{11} & m'_{33} & 0 & 0 & 0 & R' \end{bmatrix} \times \begin{Bmatrix} \varepsilon'_{11} \\ \varepsilon'_{22} \\ \varepsilon'_{33} \\ 2\varepsilon'_{23} \\ 2\varepsilon'_{13} \\ 2\varepsilon'_{12} \\ E' \end{Bmatrix}, \tag{5b}$$

with $c'_{66} = \frac{c'_{11} - c'_{12}}{2}$.

## III. THICKNESS-SHEAR VIBRATION WITH A PERFECTLY BONDED INTERFACE

First, we consider a relative simple example, i.e., the thickness-shear vibration of QCM with $u_1 = u_1(x_2, t)$,[20] in order to evaluate the properties of an additional porous layer. By using of equations motioned above, we can, respectively, deduce the governing equations in the quartz plate and porous layer

$$c_{66}u_{1,22} = \rho \ddot{u}_1, \tag{6a}$$

$$c'_{66}u'_{1,22} = \rho_0 \ddot{u}'_1, \tag{6b}$$

where the relative density is $\rho_0 = \rho_{11} - \frac{\rho_{12}^2}{\rho_{22}}$, and the fluid phase displacement satisfies $U'_1 = -\frac{\rho_{12}}{\rho_{22}}u'_1$. The solutions can be easily obtained as follows:

$$u_1 = [A\cos(\alpha x_2) + B\sin(\alpha x_2)]\exp(i\omega t), \tag{7a}$$

$$u'_1 = \left[A'\cos(\alpha' x_2) + B'\sin(\alpha' x_2)\right]\exp(i\omega t), \tag{7b}$$

where $\alpha = \frac{\omega}{\sqrt{c_{66}/\rho}}$ and $\alpha' = \frac{\omega}{\sqrt{c'_{66}/\rho_0}}$ are wavenumbers in the quartz plate and porous layer. Hence, the corresponding non-trivial stress components are, respectively,

$$T_{12} = c_{66}\alpha[-A\ \sin(\alpha x_2) + B\cos(\alpha x_2)]\exp(i\omega t), \tag{8a}$$

$$T'_{12} = c'_{66}\alpha'\left[-A'\ \sin(\alpha' x_2) + B'\cos(\alpha' x_2)\right]\exp(i\omega t). \tag{8b}$$

The top of the porous layer and bottom of quartz plate are traction free, and the displacement and stress components cross the perfect interface at $x_2 = h$ are continuous, which indicates the following relations:[21,22]

$$x_2 = h + 2h_0 : T'_{12} = 0, \tag{9}$$

$$x_2 = -h : T_{12} = 0, \tag{10}$$

$$x_2 = h : T'_{12} = T_{12}, \quad u'_1 = u_1. \tag{11}$$

Substituting Eqs. (7) and (8) into the above boundary conditions, i.e., Eqs. (9), (10), and (11), yields four linear homogeneous algebraic equations for coefficients $A$, $B$, $A'$, and $B'$

$$\begin{aligned} &-A' \sin\left[\alpha'(h+2h_0)\right] + B' \cos\left[\alpha'(h+2h_0)\right] = 0, \\ &c_{66}\alpha[-A\sin(\alpha h) + B\cos(\alpha h)] \\ &\quad = c'_{66}\alpha'[-A'\sin(\alpha' h) + B'\cos(\alpha' h)], \\ &A\cos(\alpha h) + B\sin(\alpha h) = A'\cos(\alpha' h) + B'\sin(\alpha' h), \\ &A\sin(\alpha h) + B\cos(\alpha h) = 0. \end{aligned} \tag{12}$$

The determinant of the coefficient matrix of Eq. (12) for non-trivial solutions should disappear, which leads to the following dispersion relation:

$$c_{66}\alpha \tan(2\alpha h) + c'_{66}\alpha' \tan(2\alpha' h_0) = 0. \tag{13}$$

If there is no additional porous layer exists, i.e., $h_0 = 0$, the frequency of thickness-shear vibration of quartz plate is $\omega = \frac{m\pi}{2h}\sqrt{\frac{c_{66}}{\rho}}$, $(m = 0, 1, 2, \ldots)$ with upper and bottom surfaces traction free. Once an additional porous layer is imposed on the surface of the crystal plate, its resonance frequency will be changed, which can be calculated according to Eq. (13). Comparing the two different values, we can make use of the frequency shift caused by the additional porous layer to evaluate some properties, for instance, the thickness $h_0$, elastic constant $c'_{66}$, and relative density $\rho_0$. The present contribution mainly aims to reveal the effect of imperfect interface on the performance of QCM. Detecting the properties of an additional porous layer by using of frequency shift is not our emphasis, which will not be discussed for the time being for simplification. The relatively similar proceeding can be found in the work by Yang and colleagues.[20,23]

## IV. ANTI-PLANE VIBRATION FOR AN INFINITE PLATE

The SH or anti-plane motions with only one displacement component are allowed by the linear theory of anisotropic elasticity without loss of any generality, and the motion mode in Figure 1 can then be represented by the following displacement components:[18,21,22]

$$u_1 = u_1(x_2, x_3, t), \quad u_2 = u_3 = 0, \tag{14a}$$

$$\begin{aligned} &u'_1 = u'_1(x_2, x_3, t), \quad u'_2 = u'_3 = 0, \quad U'_1 = U'_1(x_2, x_3, t), \\ &U'_2 = U'_3 = 0. \end{aligned} \tag{14b}$$

Therefore, in the linear theory of elasticity, the corresponding stresses are represented as follows:[16]

$$T_{13} = c_{55}u_{1,3} + c_{56}u_{1,2}, \quad T_{12} = c_{56}u_{1,3} + c_{66}u_{1,2}, \tag{15a}$$

$$T'_{13} = c'_{44}u'_{1,3}, \quad T'_{12} = c'_{66}u'_{1,2}. \tag{15b}$$

Based on these relations, the governing equations in the quartz plate and porous layer can be obtained as follows:[16,22,24]

$$c_{66}u_{1,22} + c_{55}u_{1,33} + 2c_{56}u_{1,23} = \rho\ddot{u}_1, \tag{16a}$$

$$\begin{aligned} &c'_{66}u'_{1,22} + c'_{44}u'_{1,33} = \rho_{11}\ddot{u}'_1 + \rho_{12}\ddot{U}'_1, \\ &\rho_{12}\ddot{u}'_1 - \rho_{22}\ddot{U}'_1 = 0. \end{aligned} \tag{16b}$$

### A. Solution of the quartz plate

Given the presence of $c_{56}$ and the related mixed derivative term, solutions to Eq. (16a) cannot be obtained in a simple and elegant manner by, e.g., the standard method of separation of variables. Mindlin[12,13] once constructed a wave solution to Eq. (16a), which is particularly useful and convenient for the present problem, i.e.,

$$u_1 = [A\cos(\eta x_2) + B\sin(\eta x_2)]\cos\left[\xi\left(\frac{c_{56}}{c_{66}}x_2 - x_3\right)\right]\exp(i\omega t), \tag{17}$$

where $A$ and $B$ are the undermined constants; $\omega$ is the frequency; and $\eta$ and $\xi$ are the wavenumbers in the $x_2$ and $x_3$ directions, respectively. Equation (17) satisfies Eq. (16a), which requires

$$\eta = \sqrt{\frac{\omega^2}{v_s^2} - \xi^2\frac{\gamma_{55}}{c_{66}}} = \frac{\pi}{2h}\sqrt{\frac{\omega^2}{\omega_s^2} - \frac{\gamma_{55}}{c_{66}}\left(\frac{2h\xi}{\pi}\right)^2}, \tag{18}$$

with $v_s = \sqrt{\frac{c_{66}}{\rho}}$, $\omega_s = \frac{\pi}{2h}v_s$, and $\gamma_{55} = c_{55} - \frac{c_{56}^2}{c_{66}}$. Thus, the shear stress component that will be needed in the boundary and continuity conditions is given by

$$\begin{aligned} T_{12} = {} & c_{66}\eta[-A\sin(\eta x_2) + B\cos(\eta x_2)] \\ & \times \cos\left[\xi\left(\frac{c_{56}}{c_{66}}x_2 - x_3\right)\right]\exp(i\omega t). \end{aligned} \tag{19}$$

### B. Solution of the porous layer

The governing equations of transversely isotropic porous layer, i.e., Eq. (16b) can be abbreviated as follows:

$$u'_{1,22} + \frac{c'_{44}}{c'_{66}}u'_{1,33} = \frac{\rho_0}{c'_{66}}\ddot{u}'_1. \tag{20}$$

Similarly, the solution can be easily obtained as follows:

$$u'_1 = \left[C\cos(\eta' x_2) + D\sin(\eta' x_2)\right]\cos\left[\xi\left(\frac{c_{56}}{c_{66}}h - x_3\right)\right]\exp(i\omega t), \tag{21}$$

where $C$ and $D$ are the undermined constants, and the wavenumbers $\xi$ and $\eta'$ satisfy the following relation:

$$\eta' = \sqrt{\frac{\omega^2}{v_0^2} - \xi^2 \frac{c'_{44}}{c'_{66}}} = \frac{\pi}{2h_0}\sqrt{\frac{\omega^2}{\omega_0^2} - \frac{c'_{44}}{c'_{66}}\left(\frac{2h_0\xi}{\pi}\right)^2}, \quad (22)$$

with $v_0 = \sqrt{\frac{c'_{66}}{\rho_0}}$ and $\omega_0 = \frac{\pi}{2h_0}v_0$. Similarly, the corresponding shear stress component in the porous layer is represented as follows:

$$T'_{12} = c'_{66}\eta'\left[-C\sin(\eta' x_2) + D\cos(\eta' x_2)\right] \times \cos\left[\xi\left(\frac{c_{56}}{c_{66}}h - x_3\right)\right]\exp(i\omega t). \quad (23)$$

### C. Boundary conditions and frequency equation

For the imperfect interface at $x_2 = h$, the classical shear-lag model was utilized to simulate its effect, i.e.,[14,15,24,25]

$$T'_{12} = T_{12} = K\left(u'_1 - u_1\right), \quad (24)$$

where the tangential displacement at this interface may be different from both sides of the interface to account for the deformation of the interface. When $K = 0$, the two parts lose their mechanical interaction, and the case of $K = \infty$ is for the perfect interface with continuous displacement across the joint.[14,15,24,25] Substituting the displacement and stress expressions, i.e., Eqs. (17), (19), (21), and (23), into the above boundary conditions, i.e., Eqs. (9), (10), and (24), yields four linear homogeneous algebraic equations for coefficients $A$, $B$, $C$, and $D$.

$$\begin{aligned} &-C\sin\left[\eta'(h+2h_0)\right] + D\cos\left[\eta'(h+2h_0)\right] = 0,\\ &c_{66}\eta[-A\sin(\eta h) + B\cos(\eta h)]\\ &\quad = c'_{66}\eta'[-C\sin(\eta' h) + D\cos(\eta' h)],\\ &c_{66}\eta[-A\sin(\eta h) + B\cos(\eta h)]\\ &\quad = K\left[C\cos(\eta' h) + D\sin(\eta' h) - A\cos(\eta h) - B\sin(\eta h)\right],\\ &A\sin(\eta h) + B\cos(\eta h) = 0. \end{aligned} \quad (25)$$

The determinant of the coefficient matrix for non-trivial solutions should disappear, which leads to the following dispersion relation that determines the frequency for SH vibration:

$$\frac{c'_{66}\eta'}{c_{66}\eta}\tan(2\eta' h_0)[1 - \Gamma\eta h\tan(2\eta h)] + \tan(2\eta h) = 0, \quad (26)$$

in which the non-dimensional number $\Gamma = \frac{c_{66}}{Kh}$ describes how well the porous layer and quartz plate are bonded. If the interface is perfect, i.e., $\Gamma = 0$, Eq. (26) can be reduced as follows:

$$\frac{c'_{66}\eta'}{c_{66}\eta}\tan(2\eta' h_0) + \tan(2\eta h) = 0, \quad (27)$$

which has similar expression as that of Lee and Chang.[26]

Furthermore, when no additional porous layer exists, i.e., $h_0 = 0$, $2\eta h = m\pi$ can be obtained for different branches $m = 0, 1, 2, \ldots$. Hence,

$$\Omega = \sqrt{m^2 + Z^2}, \quad (28)$$

where $\Omega = \frac{\omega}{\omega_s}$ and $Z = \sqrt{\frac{\gamma_{55}}{c_{66}}}\left(\frac{2h\xi}{\pi}\right)$. Equation (28) is the resonance frequency of the anti-plane vibration for a free infinite AT-cut quartz plate solved by Mindlin.[12]

### D. Effect of the imperfect interface on the face shear wave (m = 0)

Figure 2 shows the dispersion curves of a free infinite AT-cut quartz plate without additional mass layer, as previously depicted by previous researchers.[12,27] The case of $m = 0$ is the face shear wave, which is a straight line going through the origin and is non-dispersive. The waves corresponding to the curves of $m \neq 0$ are the thickness twist waves, which are dispersive. The finite intercepts with the $\Omega$ axis are the cutoff frequencies; below which, the wavenumber becomes pure imaginary and the corresponding waves cannot propagate.

As a special case, the effect of imperfect interface on the face shear wave ($m = 0$) is considered in the following presentation. For mass loading sensors or QCM, the coating porous layers are usually very thin ($2h_0 \ll 2h$); thus, the following approximations can be made:[28]

$$\tan(2\eta' h_0) = 2\eta' h_0. \quad (29)$$

For the lowest mode of a bare AT-cut quartz plate, $2\eta h = 0$. For the composite structure shown in Figure 1, the effect of this additional porous layer can be regarded as a perturbation.[28] Putting $2\eta h = \delta$ and using the fact that $\delta$ is a very small quantity, then

$$\frac{v_0^2}{v_s^2}\frac{2\rho_0 h_0}{2\rho h}\eta'^2\left[1 - 2\Gamma(\eta h)^2\right] + \eta^2 = 0. \quad (30)$$

When the interface is perfect, i.e., $\Gamma = 0$, Eq. (30) is a linear equation with only one unknown. Thus, the frequency expression can be obtained as follows:

$$\Omega = \sqrt{\frac{1 + \frac{v_0^2}{v_s^2}\frac{2\rho_0 h_0}{2\rho h}\frac{c'_{44}/c'_{66}}{\gamma_{55}/c_{66}}}{1 + \frac{2\rho_0 h_0}{2\rho h}}}Z, \quad (31)$$

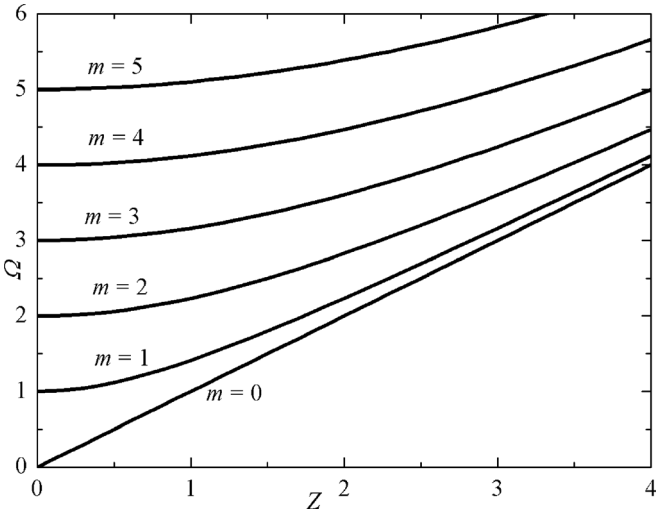


FIG. 2. Dispersion curves of infinite AT-cut quartz plate with an additional layer.

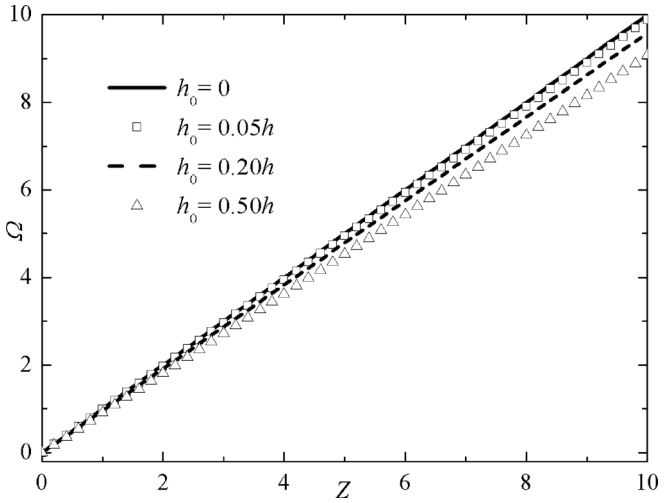


FIG. 3. Dispersive relationship of face shear wave for some selected thickness of the porous layer with a perfect interface ($m = 0$ and $\Gamma = 0$).

which determines the frequency of the face shear wave when the infinite AT-cut quartz plate is covered by a transversely isotropic porous layer. Both the stiffness and inertia of the porous layer are included in present discussion. Figure 3 shows the frequency branches for different thicknesses of the additional layer, with $\frac{c'_{44}}{c'_{66}} = 1$ and $\rho_0 = 1500\,\mathrm{kg/m^3}$. The curve is also a straight line going through the origin for different conditions. Thicker porous layer lowers the frequency and slope, as shown in Figure 3.

For the imperfect interface ($\Gamma \neq 0$), Eq. (30) is a quadratic equation with one unknown $\Omega^2$. With the introduction of non-dimensional variables $R = \frac{2\rho_0 h_0}{2\rho h}$ and $T = \frac{v_0^2}{v_s^2}\frac{c'_{44}/c'_{66}}{\gamma_{55}/c_{66}}$, Eq. (30) can be reduced as follows:

$$\frac{\pi^2\Gamma R}{2}\Omega^4 - \left[R + \frac{\pi^2\Gamma R}{2}(T+1)Z^2 + 1\right]\Omega^2 + \left(\frac{\pi^2\Gamma RT}{2}Z^2 + RT + 1\right)Z^2 = 0. \tag{32}$$

Assuming $M = \frac{\pi^2\Gamma R}{2}$, $N = R + \frac{\pi^2\Gamma R}{2}(T+1)Z^2 + 1$, and $Q = \left(\frac{\pi^2\Gamma RT}{2}Z^2 + RT + 1\right)Z^2$, the frequency solution can be written as follows:

$$\Omega_1 = \left(\frac{N - \sqrt{N^2 - 4MQ}}{2M}\right)^{\frac{1}{2}}, \quad \Omega_2 = \left(\frac{N + \sqrt{N^2 - 4MQ}}{2M}\right)^{\frac{1}{2}}. \tag{33}$$

Two resonance frequencies are available for imperfect interfaces, which is totally different from the perfect case, i.e., Eq. (31). By calculating the values, we can calculate that $\Omega_1$ corresponds to face shear wave, and $\Omega_2$ is the new thickness twist mode with a cutoff frequency, which is excited by the imperfect interface. When $\Gamma = 0$, $\Omega_2$ disappears, and $\Omega_1$ is equal to $\Omega$ in Eq. (31).

Figure 4 shows the dispersive relationship when the upper porous layer is imperfectly bonded on the infinite AT-cut quartz plate ($m = 0$). The red curve has a finite intercept with the frequency axis. These intercepts are called cutoff

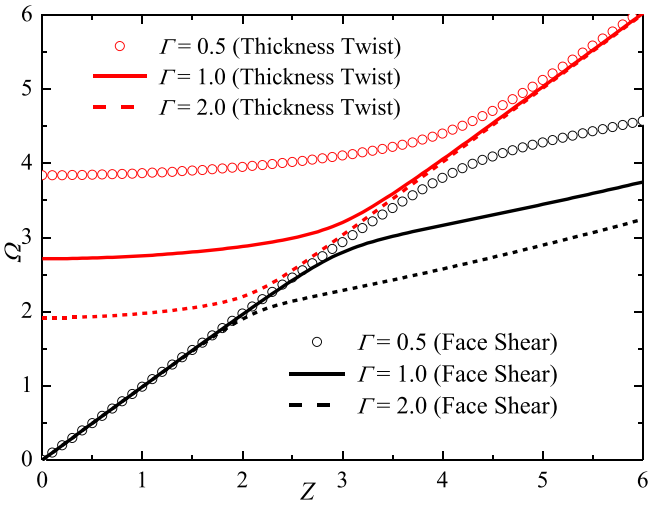


FIG. 4. Dispersive relationship of the face shear wave when the upper porous layer is imperfectly bonded on the infinite AT-cut quartz plate ($m = 0$): (a) $h_0 = h/20$; (b) $h_0 = h/5$.

frequencies, below which, the wavenumber becomes pure imaginary and the corresponding waves cannot propagate. The appearance of this new thickness twist wave caused by weak interfaces is qualitatively different from a classical composite plate with perfect interfaces. When $K$ decreases or $\Gamma$ increases, the interface bonding becomes weaker and the frequencies of the waves become lower as expected. In addition, the face shear branch when $\Gamma \neq 0$ is linear only at a certain region. For example, these curves are kept straight

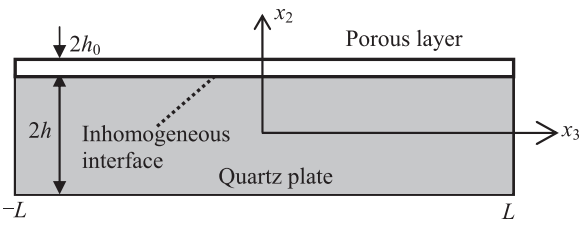


FIG. 5. A QCM with an inhomogeneous interface between the porous layer and the AT-cut quartz plate.

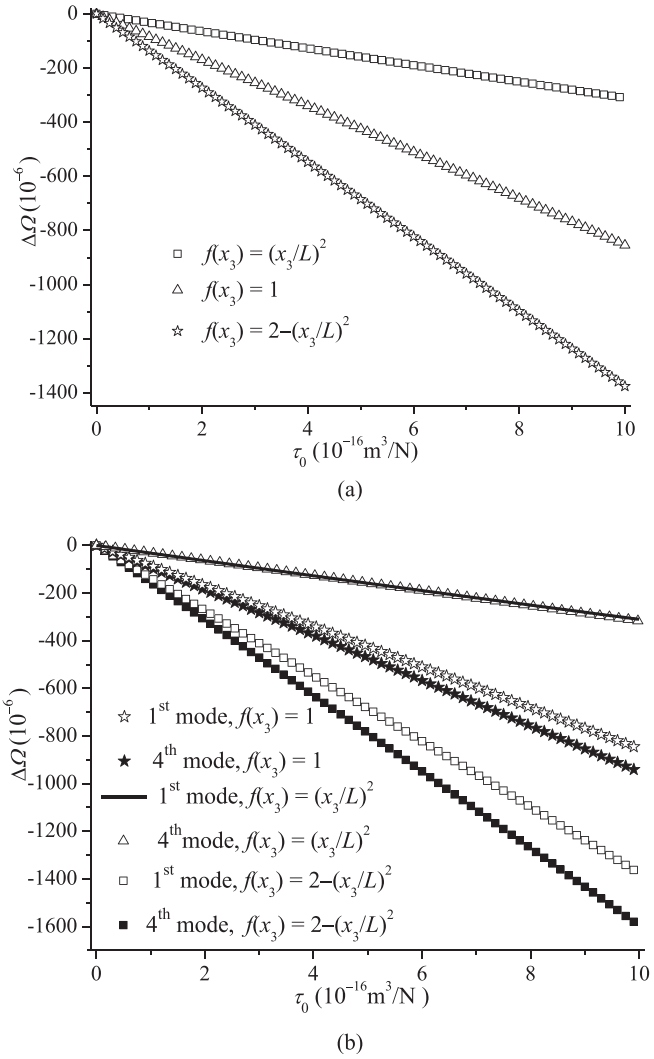


FIG. 6. Non-dimensional frequency shift caused by different interfaces: (a) First mode; (b) comparison for different modes.

in the region $Z < 2$ for $h_0 = h/20$. With the increase in the thickness of the porous layer, the linear region narrows, i.e., $Z < 1$ for $h_0 = h/5$, as shown in Figure 4(b).

## V. EFFECT OF THE INHOMOGENEOUS INTERFACE IN A FINITE AT-CUT QUARTZ PLATE

A fully distributed porous layer imperfectly embedded in a finite AT-cut quartz plate is considered in this study, as shown in Figure 5. The pure anti-plane vibration can be separated in the composite structure by properly choosing the plate aspect ratio, i.e., length/thickness.[27] Furthermore, in realistic situations, the contact between two parts can be non-uniform and, most probably, weaker at the corners of the plate edges.[29] To examine the effect of such inhomogeneous interface stiffness distributions, the interface is considered as functional graded, that is, the interface parameter gradually changes along plate length direction.

### A. Solution of the quartz plate

For the AT-cut quartz plates, $c_{55} = 68.81$ GPa, $c_{56} = 2.53$ GPa, and $c_{66} = 29.01$ GPa.[16] The value of $c_{56}$ is very small compared with $c_{55}$ and $c_{66}$, therefore, the usual approximation of neglecting the small $c_{56}$ is followed throughout the rest of the equations discussed in this article.[14,27] Based on this assumption, the governing field equation can be abbreviated as follows:

$$u_{1,22} + \frac{c_{55}}{c_{66}} u_{1,33} = \frac{\rho}{c_{66}} \ddot{u}_1. \tag{34}$$

The solution can be obtained by expanded trigonometric function along the $x_3$ direction.[14,27] Hereafter, $\exp(i\omega t)$ is omitted for brevity

$$u_1 = [A_0 \cos(\eta_0 x_2) + B_0 \sin(\eta_0 x_2)] + \sum_{n=1,2,3,\ldots}^{\infty} [A_n \cos(\eta_n x_2) + B_n \sin(\eta_n x_2)] \cos(\alpha_n x_3), \tag{35}$$

where $A_0$, $B_0$, $A_n$, and $B_n$ are the undetermined constants, and $T_{13} = 0$ at $x_3 = \pm L$ is satisfied when $\alpha_p = \frac{p\pi}{L}$, $(p = 0, 1, 2, \ldots)$. In this equation, only the cosine series solution in the $x_3$ direction is considered for simplification. Equation (35) satisfies (34) when

$$\eta_p^2 = \frac{\pi^2}{4h^2} \left[ \frac{\omega^2}{\omega_s^2} - \frac{c_{55}}{c_{66}} \left( p \frac{2h}{L} \right)^2 \right], \ (p = 0, 1, 2, \ldots). \tag{36}$$

The shear stress component, which will be used in the subsequent boundary conditions, is given by

$$T_{12} = c_{66} \left\{ \eta_0 [-A_0 \sin(\eta_0 x_2) + B_0 \cos(\eta_0 x_2)] + \sum_{n=1,2,3,\ldots}^{\infty} \eta_n [-A_n \sin(\eta_n x_2) + B_n \cos(\eta_n x_2)] \cos(\alpha_n x_3) \right\}. \tag{37}$$

### B. Solution of porous layer

Similarly, the solution of Eq. (20) can be obtained using the trigonometric function expansion technique

$$u_1' = \left[ A_0' \cos(\eta_0' x_2) + B_0' \sin(\eta_0' x_2) \right] + \sum_{m=1,2,3,\ldots}^{\infty} \left[ A_m' \cos(\eta_m' x_2) + B_m' \sin(\eta_m' x_2) \right] \cos(\alpha_m x_3), \tag{38}$$

where $A_0'$, $B_0'$, $A_n'$, and $B_n'$ are the undetermined constants, and $T_{13}' = 0$ at $x_3 = \pm L$ is satisfied. Equation (38) needs to satisfy Eq. (20), which requires

$$\eta_p'^2 = \frac{\pi^2}{4h_0^2} \left[ \frac{\omega^2}{\omega_0^2} - \frac{c_{44}'}{c_{66}'} \left( p \frac{2h_0^2}{L} \right)^2 \right], \quad (p = 0, 1, 2, \ldots). \tag{39}$$

The corresponding stress component $T_{12}'$ is

$$T_{12}' = c_{66}' \left\{ \eta_0' [-A_0' \sin(\eta_0' x_2) + B_0' \cos(\eta_0' x_2)] + \sum_{m=1,2,3,\ldots}^{\infty} \eta_m' [-A_m' \sin(\eta_m' x_2) + B_m' \cos(\eta_m' x_2)] \cos(\alpha_m x_3) \right\}. \tag{40}$$

### C. Boundary conditions and frequency equation

The top and bottom boundary conditions are the same as those in Eqs. (9) and (10). Instead of the stiffness coefficient, the interface flexibility coefficient was used to simulate the effect of the inhomogeneous interface at $x_2 = h$[30]

$$\tau T'_{12} = \tau T_{12} = u'_1 - u_1, \tag{41}$$

where $\tau = \frac{1}{K}$ describes how well the two portions are bonded. Simultaneously, we regard this equation as a function of $x_3$, i.e., $\tau = \tau_0 f(x_3)$. Substituting Eqs. (35), (37), (38), and (40) into the boundary conditions Eqs. (9), (10) and (41) yields

$$\begin{aligned}&\eta'_0\{-A'_0\sin[\eta'_0(h+2h_0)] + B'_0\cos[\eta'_0(h+2h_0)]\}\\&+\sum_{m=1,2,3,\ldots}^{\infty}\eta'_m\{-A'_m\sin[\eta'_m(h+2h_0)] + B'_m\cos[\eta'_m(h+2h_0)]\}\cos(\alpha_m x_3) = 0,\end{aligned} \tag{42a}$$

$$\begin{aligned}&\frac{c'_{66}}{c_{66}}\left\{\eta'_0[-A'_0\sin(\eta'_0 h) + B'_0\cos(\eta'_0 h)] + \sum_{m=1,2,3,\ldots}^{\infty}\eta'_m[-A'_m\sin(\eta'_m h) + B'_m\cos(\eta'_m h)]\cos(\alpha_m x_3)\right\}\\&= \eta_0[-A_0\sin(\eta_0 h) + B_0\cos(\eta_0 h)] + \sum_{n=1,2,3,\ldots}^{\infty}\eta_n[-A_n\sin(\eta_n h) + B_n\cos(\eta_n h)]\cos(\alpha_n x_3),\end{aligned} \tag{42b}$$

$$\begin{aligned}&[A'_0\cos(\eta'_0 h) + B'_0\sin(\eta'_0 h) - A_0\cos(\eta_0 h) - B_0\sin(\eta_0 h)] + \sum_{m=1,2,3,\ldots}^{\infty}[A'_m\cos(\eta'_m h) + B'_m\sin(\eta'_m h)]\cos(\alpha_m x_3)\\&-\sum_{n=1,2,3,\ldots}^{\infty}[A_n\cos(\eta_n h) + B_n\sin(\eta_n h)]\cos(\alpha_n x_3)\\&= \tau_0 f(x_3)c_{66}\left\{\eta_0[-A_0\sin(\eta_0 h) + B_0\cos(\eta_0 h)] + \sum_{n=1,2,3,\cdots}^{\infty}\eta_n[-A_n\sin(\eta_n h) + B_n\cos(\eta_n h)]\cos(\alpha_n x_3)\right\},\end{aligned} \tag{42c}$$

$$\eta_0[A_0\sin(\eta_0 h) + B_0\cos(\eta_0 h)] + \sum_{n=1,2,3,\ldots}^{\infty}\eta_n[A_n\sin(\eta_n h) + B_n\cos(\eta_n h)]\cos(\alpha_n x_3) = 0. \tag{42d}$$

Multiplying Eqs. (42) by $\cos(\alpha_p x_3)$ for $p = 0, 1, 2, \ldots$, respectively, and integrating the resulting equations from $-L$ to $L$, the following linear equations for the undetermined constants are obtained:

$$\begin{aligned}-A'_0\sin[\eta'_0(h+2h_0)] + B'_0\cos[\eta'_0(h+2h_0)] &= 0,\\-A'_m\sin[\eta'_m(h+2h_0)] + B'_m\cos[\eta'_m(h+2h_0)] &= 0,\end{aligned} \tag{43a}$$

$$\begin{aligned}\eta_0[-A_0\sin(\eta_0 h) + B_0\cos(\eta_0 h)] &= \frac{c'_{66}}{c_{66}}\eta'_0[-A'_0\sin(\eta'_0 h) + B'_0\cos(\eta'_0 h)],\\\eta_n[-A_n\sin(\eta_n h) + B_n\cos(\eta_n h)] &= \frac{c'_{66}}{c_{66}}\eta'_n[-A'_n\sin(\eta'_n h) + B'_n\cos(\eta'_n h)],\end{aligned} \tag{43b}$$

$$\begin{aligned}&A'_0\cos(\eta'_0 h) + B'_0\sin(\eta'_0 h) - A_0\cos(\eta_0 h) - B_0\sin(\eta_0 h)\\&= \frac{c_{66}\tau_0}{2L}\left\{\eta_0[-A_0\sin(\eta_0 h) + B_0\cos(\eta_0 h)]\int_{-L}^{L}f(x_3)dx_3 + \sum_{n=1,2,3,\ldots}^{\infty}\eta_n[-A_n\sin(\eta_n h) + B_n\cos(\eta_n h)]\int_{-L}^{L}f(x_3)\cos(\alpha_n x_3)dx_3\right\},\\&A'_m\cos(\eta'_m h) + B'_m\sin(\eta'_m h) - A_m\cos(\eta_m h) - B_m\sin(\eta_m h)\\&= \frac{c_{66}\tau_0}{L}\left\{\eta_0[-A_0\sin(\eta_0 h) + B_0\cos(\eta_0 h)]\int_{-L}^{L}f(x_3)\cos(\alpha_m x_3)dx_3\right.\\&\left.+\sum_{n=1,2,3,\ldots}^{\infty}\eta_n[-A_n\sin(\eta_n h) + B_n\cos(\eta_n h)]\int_{-L}^{L}f(x_3)\cos(\alpha_n x_3)\cos(\alpha_m x_3)dx_3\right\},\end{aligned} \tag{43c}$$

$$\begin{aligned}-A_0\sin(\eta_0 h) + B_0\cos(\eta_0 h) &= 0,\\-A_n\sin(\eta_n h) + B_n\cos(\eta_n h) &= 0.\end{aligned} \tag{43d}$$

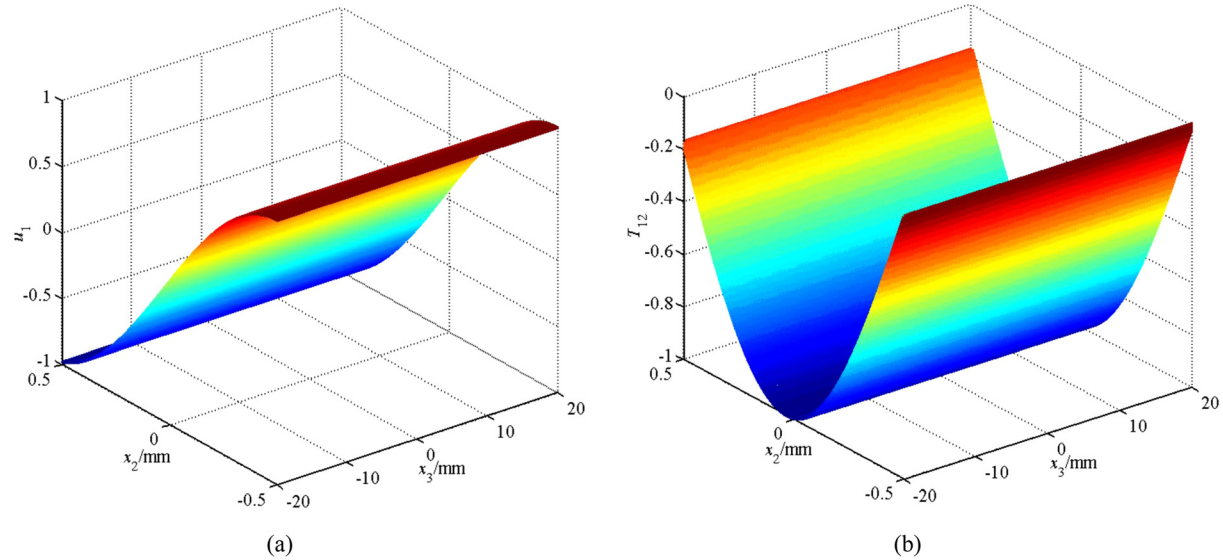


FIG. 7. Relative displacement and stress distributions of the first mode of the quartz plate with a homogeneous interface ($f(x_3) = 1$, $\tau_0 = 1 \times 10^{-15}\text{m}^3/\text{N}$): (a) Relative displacement $u_1$; (b) relative stress $T_{12}$.

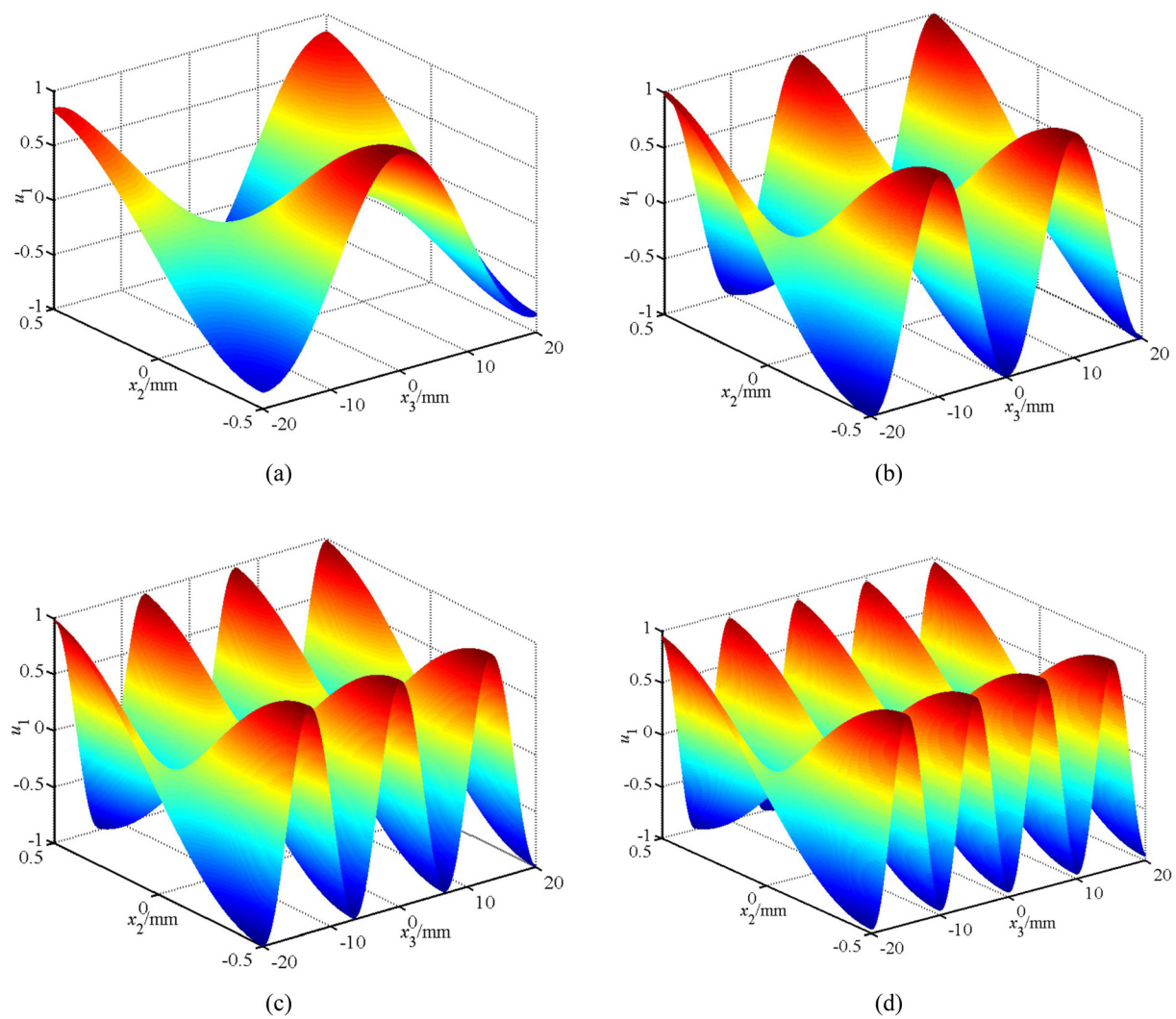


FIG. 8. Relative displacement $u_1$ of the first four symmetric modes of QCM with an inhomogeneous interface ($f(x_3) = 2 - \left(\frac{x_3}{L}\right)^2$, $\tau_0 = 1 \times 10^{-15}\text{m}^3/\text{N}$): (a) First mode ($\Omega_1 = 0.94340825$); (b) second mode ($\Omega_2 = 0.95176225$); (c) third mode ($\Omega_3 = 0.96558775$); (d) fourth mode ($\Omega_4 = 0.98461075$).

For the non-trivial solutions, the determinant of the coefficient matrix has to vanish, and the frequency can then be obtained.

### D. Numerical simulation

For a numerical example, an AT-cut quartz plate, with half length of $L = 20\,\text{mm}$, thickness of $2h = 1\,\text{mm}$, and mass density of the plate $\rho = 2649\,\text{kg/m}^3$, is considered. The following parameters are used for the porous layer:[31] $c'_{44} = 7.5\,\text{GPa}$, $c'_{66} = 5.535\,\text{GPa}$, $\rho_0 = 1500\,\text{kg/m}^3$, and $h_0 = 0.1\,h$. Equation (43) is a transcendental equation, in which the frequency cannot be solved using an explicit expression. Thus, the following iterative procedure was adopted for numerical computations.[32] For an initial value of $\omega$, the determinant of the coefficient matrix, presented in the left hand of Eq. (43), was evaluated, and a fixed but small increment was added to the frequency until the value of the determinant changed its sign. The "bisection method" was then applied to locate the root correction to a chosen number of decimal places. In the following discussion, this study mainly focuses on the energy trapping phenomenon, i.e., $(1-R) < \Omega < 1$ for the uniform porous layer.[12,14,15] Meanwhile, three different kinds of interfaces were adopted as follows:

$$f_0(x_3) = 1, \quad f_1(x_3) = \left(\frac{x_3}{L}\right)^2, \quad f_2(x_3) = 2 - \left(\frac{x_3}{L}\right)^2. \quad (44)$$

$f_0(x_3) = 1$ is the homogeneous weak interface. $f_1(x_3) = \left(\frac{x_3}{L}\right)^2$ is related to the case that the interface is weaker at the corners of the plate edges and the porous layer perfectly bonded at the crystal plate center. $f_2(x_3) = 2 - \left(\frac{x_3}{L}\right)^2$ corresponds to the circumstance that the interface flexibility coefficient reaches its maximum at the center of the plate, which may be induced by local defect at $x_3 = 0$, such as the micropore or fine crack. Taking the case of $f_2(x_3) = 2 - \left(\frac{x_3}{L}\right)^2$, for example, four frequencies are always found when using 10

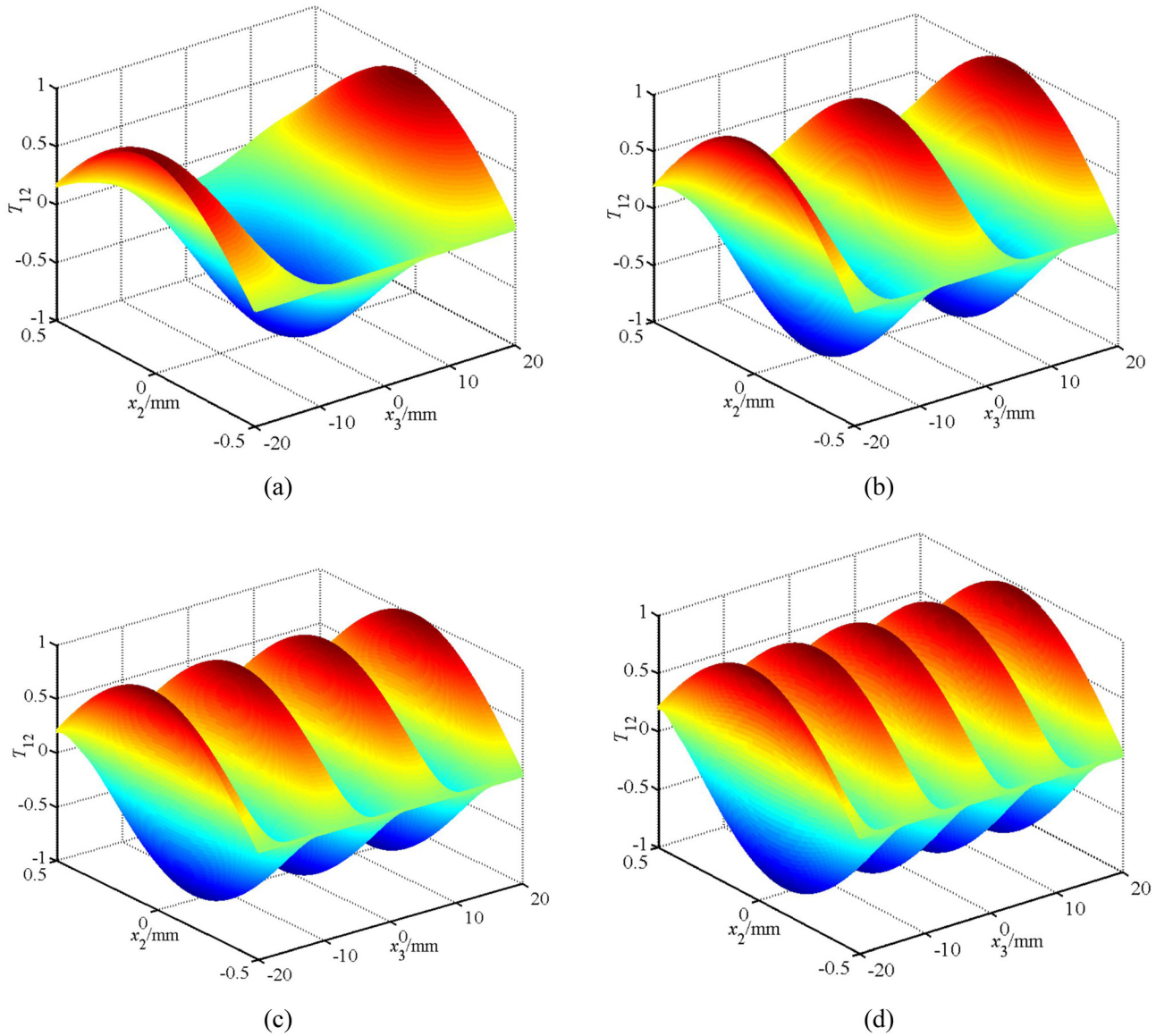


FIG. 9. Relative stress component $T_{12}$ of the first four symmetric modes of QCM with an inhomogeneous interface ($f(x_3) = 2 - \left(\frac{x_3}{L}\right)^2$, $\tau_0 = 1 \times 10^{-15}\text{m}^3/\text{N}$): (a) First mode ($\Omega_1 = 0.94340825$); (b) second mode ($\Omega_2 = 0.95176225$); (c) third mode ($\Omega_3 = 0.96558775$); (d) fourth mode ($\Omega_4 = 0.98461075$).

and 11 terms in the series: $\Omega_1 = 0.94340825$, $\Omega_2 = 0.95176225$, $\Omega_3 = 0.96558775$, and $\Omega_4 = 0.98461075$. Seven significant figures are used to ensure sufficient accuracy of the frequencies. In this case, the corresponding modes also converged well, without noticeable differences. Therefore, all calculations below are based on calculations using 10 terms in the series.

Fortunately, $\eta_p^2$ and $\eta_p'^2$ for $p = 0, 1, 2, \ldots$ is positive in this case, thereby reducing the complexity of the numerical simulation. When a large $p$ is indeed needed, $\eta_p^2$ and $\eta_p'^2$ can be redefined with a minus sign and the sine and cosine functions in Eqs. (35) and (38) can be changed to hyperbolic sine and cosine functions, respectively.[14,29]

The frequency shift can be defined as $\Delta\omega = \omega' - \bar{\omega}$, where $\omega'$ and $\bar{\omega}$ represent the frequencies of the plate when the interface is imperfect and perfect, respectively. Figure 6(a) provides the non-dimensional frequency shift $\Delta\Omega$ of the fundamental mode as a function with the interfacial flexibility coefficient $\tau_0$ for different kinds of interfaces, such as Eq. (44). The relationship between the frequency change and the interfacial parameter is linear for the homogeneous weak interface, which can be proved by Chen *et al.*,[33] and can be used to measure the level of the interface bonding. The inhomogeneity of the interface does not change its linear relationship. However, the slope has been changed because of the inconsistency of the interface. If the interface coefficient is judged according to the uniform interface, some bias error may occur. Meanwhile, higher mode has a larger frequency shift than the fundamental mode, as shown in Figure 6(b). This variation is not evident when $f(x_3) = \left(\frac{x_3}{L}\right)^2$ because this interface approaches closer to the perfect case compared with the other two cases.

In the following figures, the values of the displacement and stress components are normalized in such a way that the maximal displacement is equal to one.[14,15] When the interface is uniform, i.e., $f(x_3) = 1$, no inhomogeneous factor exists in the calculation model (Figure 5). Thus, only one term of the trigonometric function series is enough for the numerical simulation. Meanwhile, the stress and displacement distributions along the $x_3$ direction must be uniform from a physical point of view. The displacement and stress variations of the fundamental mode in the AT-cut quartz plate in Figure 7 have proven its correctness. Other higher modes have the same tendency, which are not depicted one by one. Moreover, stress $T_{12}$ remains zero at the bottom surface $x_2 = -h$, which is decided by Eq. (10), validating the accuracy of our calculation to some extent.

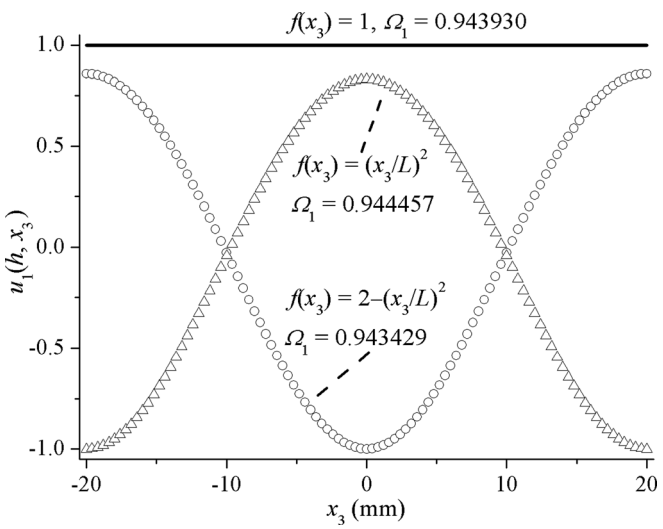


FIG. 10. Displacement comparison of the first mode along the $x_3$ direction for different interfaces ($x_2 = h$, $\tau_0 = 1 \times 10^{-15}\text{m}^3/\text{N}$).

Taking the case of $f(x_3) = 2 - \left(\frac{x_3}{L}\right)^2$ as an example, the non-uniform interface evidently changed displacement and stress distributions, as shown in Figures 8 and 9. These displacement and stress distributions are all symmetric about the $x_2$ axis because only cosine function along $x_3$ direction is considered. Along the $x_2$ direction, the displacement is anti-symmetric, whereas the stress is symmetric. The stress component remains zero at all times at $x_2 = -h$, as shown in Figure 9. The first, second, third, and fourth modes have two, four, six, and eight points with zero value along the plate length, respectively. Notably, this case is not the energy trapping phenomenon that is due to the non-zero values of displacement and stress at the edge $x_3 = \pm L$.

Figure 10 shows the displacement comparison of the first mode for the three interfaces above. Mostly, the maximum of amplitude takes place at the edges of the plate when the interface is non-uniform, such as $f(x_3) = \left(\frac{x_3}{L}\right)^2$, which can be used to explain the phenomenon that the connected portion was first isolated near the plate edge.

## VI. CONCLUSION

The solutions for the anti-plane vibration of an infinite and finite AT-cut quartz plate with transversely isotropic porous layer imperfectly bonded on its surface were obtained. Based on some simplification and perturbation solutions, a new thickness twist wave caused by the imperfect interface was revealed in an infinite crystal plate. Meanwhile, the inhomogeneity of the interface was also investigated in a finite quartz plate by the trigonometric function expansion technique. The frequency, displacement, and stress distributions changed evidently because of the non-uniform interface, which should be given more attention in sensor application.

Frankly speaking, it may be more pronounced in longitudinal modes, e.g., the thickness-extensional modes, rather than in shear modes of a plate by evaluating the porosity of the additional fluid- or air-filled solid layer according to the frequency shift of a resonator, which needs to be proved theoretically and experimentally in the near future.

## ACKNOWLEDGMENTS

The National Natural Science Foundation of China (No. 11272247) and the National 111 Project of China (No. B06024) are gratefully acknowledged for their financial support.

[1]J. G. Miller and D. I. Bolef, J. Appl. Phys. **39**, 5815 (1968).
[2]F. Lu, H. P. Lee, and S. P. Lim, Sens. Actuators A **112**, 203 (2004).
[3]A. Arnau, Sensors **8**, 370 (2008).

[4]A. Tuantranont, A. Wisitsora-At, P. Sritongkham, and K. Jaruwongrungsee, Anal. Chim. Acta **687**, 114 (2011).
[5]R. Etchenique and V. L. Brudny, Langmuir **16**, 5064 (2000).
[6]S.-H. Kim, J.-S. Lee, H.-C. Choi, and Y.-H. Lee, IEEE Electron Device Lett. **20**, 113 (1999).
[7]R. J. Lazarowich, P. Taborek, B.-Y. Yoo, and N. V. Myung, J. Appl. Phys. **101**, 104909 (2007).
[8]M. Hieda, R. Garcia, M. Dixon, T. Daniel, D. Allara, and M. H. W. Chan, Appl. Phys. Lett. **84**, 628 (2004).
[9]H. Zhuo, F. Peng, L. Lin, Y. Qu, and F. Lai, Thin Solid Films **519**, 2308 (2011).
[10]G. Z. Sauerbrey, Z. Phys. **155**, 206 (1959).
[11]J. R. Vig and A. Ballato, IEEE Trans. Ultrason. Ferroelectr. Freq. Control **45**, 1123 (1998).
[12]R. D. Mindlin, Int. J. Solids Struct. **1**, 141 (1965).
[13]R. D. Mindlin, J. Acoust. Soc. Am. **41**, 969 (1967).
[14]X. Li, Y. Wang, T. Xiao, Q. Jiang, and J. Yang, IEEE Sens. J. **13**, 574 (2013).
[15]Y. Chen, J. Du, J. Wang, and J. Yang, IEEE Trans. Ultrason. Ferroelectr. Freq. Control **58**, 616 (2011).
[16]H. F. Tiersten, *Linear Piezoelectric Plate Vibrations* (Plenum, New York, 1969).
[17]M. A. Biot, J. Acoust. Soc. Am. **28**, 168 (1956).
[18]M. S. Son and Y. J. Kang, Wave Motion **49**, 490 (2012).
[19]S. P. Joshi, Smart Mater. Struct. **1**, 80 (1992).
[20]J. Yang, H. Zhou, and W. Zhang, IEEE Trans. Ultrason. Ferroelectr. Freq. Control **52**, 918 (2005).
[21]A. Pradhan, S. K. Samal, and N. C. Mahanti, Sadhana **27**, 595 (2002).
[22]A. K. Vashishth and A. Dahiya, Acta Mech. **224**, 727 (2013).
[23]Y. Chen, J. Du, J. Wang, and J. Yang, Philos. Mag. Lett. **93**, 362 (2013).
[24]A. Melkumyan and Y. W. Mai, Philos. Mag. **88**, 2965 (2008).
[25]J. P. Jones and J. S. Whither, J. Appl. Mech. Trans. ASME **34**, 905 (1967).
[26]P. C. Y. Lee and N. Chang, J. Elasticity **9**, 51 (1979).
[27]J. Zhu, W. Chen, and J. Yang, IEEE Trans. Ultrason. Ferroelectr. Freq. Control **60**, 858 (2013).
[28]Z. Wang, C. K. Jen, and J. D. N. Cheeke, IEEE Trans. Ultrason. Ferroelectr. Freq. Control **41**, 397 (1994).
[29]N. Mori, S. Biwa, and T. Hayashi, J. Appl. Phys. **113**, 074901 (2013).
[30]M. Schoenberg, J. Acoust. Soc. Am. **68**, 1516 (1980).
[31]D. I. Fotiadis, G. Foutsitzi, and C. V. Massalas, Acta Mech. **137**, 65 (1999).
[32]A. N. Abdalla, F. Alsheikh, and A. Y. AlHossain, Mat. Sci. Eng. B-Solid. **162**, 147 (2009).
[33]J. Chen, W. Wang, J. Wang, Z. Yang, and J. Yang, IEEE Trans. Ultrason. Ferroelectr. Freq. Control **55**, 1678 (2008).